Singular value decomposition of a dual orthogonal-view polarized fluorescence microscope

Talon Chandler, Min Guo, Hari Shroff, Rudolf Oldenbourg, Patrick La Rivière

July 12, 2018

1 Introduction

In these notes we will find the kernel, transfer function, and singular value decomposition of a dual orthogonal view polarized fluorescence microscope (diSPIM). We will model the relationship between the spatio-angular density of fluorophores in a three-dimensional sample—a member of $\mathbb{L}_2(\mathbb{R}^3 \times \mathbb{S}^2)$—and the two three-dimensional volumes for each illumination polarization setting—two members of $\mathbb{L}_2(\mathbb{R}^3 \times \mathbb{S}^1)$. We could consider the diSPIM as a microscope that makes two samples of a larger space $\mathbb{L}_2(\mathbb{R}^3 \times \mathbb{S}^1 \times \mathbb{S}^2)$, but I don't think this will give us any extra insight at this point.

We can write the forward model for the polarized diSPIM as

$$g_{\mathrm{v}}(\mathfrak{r}_d, \hat{\mathbf{p}}) = [\mathcal{H}f]_{\mathrm{v}}(\mathfrak{r}_d, \hat{\mathbf{p}}) = \int_{\mathbb{R}^3} d\mathfrak{r}_o \int_{\mathbb{S}^2} d\hat{\mathbf{s}}_o \, h_{\mathrm{v}}(\mathfrak{r}_d - \mathfrak{r}_o, \hat{\mathbf{p}}, \hat{\mathbf{s}}_o) f(\mathfrak{r}_o, \hat{\mathbf{s}}_o), \tag{1}$$

where $\mathrm{v} \in \{\mathrm{A}, \mathrm{B}\}$ is the light path index, $\mathfrak{r}_d$ is the three-dimensional detection coordinate, and all other coordinates have been introduced in previous note sets. The adjoint operator is given by

$$f(\mathfrak{r}_o, \hat{\mathbf{s}}_o) = [\mathcal{H}^\dagger \mathbf{g}](\mathfrak{r}_o, \hat{\mathbf{s}}_o) = \sum_{\mathrm{v} \in \{\mathrm{A},\mathrm{B}\}} \int_{\mathbb{R}^3} d\mathfrak{r}_d \int_{\mathbb{S}^1} d\hat{\mathbf{p}} \, h_{\mathrm{v}}(\mathfrak{r}_d - \mathfrak{r}_o, \hat{\mathbf{p}}, \hat{\mathbf{s}}_o) g_{\mathrm{v}}(\mathfrak{r}_d, \hat{\mathbf{p}}). \tag{2}$$

2 Kernel

The polarized diSPIM illuminates the sample with a uniform-width Gaussian beam (we ignore light-sheet broadening) with variable polarization. In path A the light sheet is in the xy plane for viewing by an objective with an optical axis along the z axis. In path B the roles are reversed and the light sheet is in the yz plane for viewing by an objective with an optical axis along the x axis.

In the May 14 notes we derived the excitation kernel for a polarized collimated beam (NA = 0) traveling along the z axis. The excitation kernel for path B of the diSPIM is identical to the previously derived excitation kernel weighted by Gaussian profile of the light sheet

$$h_{\mathrm{B,exc}}(\mathfrak{r}_o, \hat{\mathbf{s}}_o; \hat{\mathbf{p}}) = \left[z_0^{\mathrm{B}}(\hat{\mathbf{p}}) y_0^0(\hat{\mathbf{s}}_o) + \sqrt{\frac{3}{5}} z_{-2}^{\mathrm{B}}(\hat{\mathbf{p}}) y_2^{-2}(\hat{\mathbf{s}}_o) - \frac{1}{\sqrt{5}} z_0^{\mathrm{B}}(\hat{\mathbf{p}}) y_2^0(\hat{\mathbf{s}}_o) + \sqrt{\frac{3}{5}} z_2^{\mathrm{B}}(\hat{\mathbf{p}}) y_2^2(\hat{\mathbf{s}}_o) \right] \mathfrak{g}(r_x, \sigma_{\mathrm{ls}}), \tag{3}$$

where $\mathfrak{g}(x, \sigma) \equiv \exp(x^2/2\sigma^2)/\sqrt{2\pi\sigma^2}$, $\mathfrak{r}_o = r_x\hat{\mathbf{x}} + r_y\hat{\mathbf{y}} + r_z\hat{\mathbf{z}}$ is the three-dimensional position vector in the object, and σ_{ls} is the spatial standard deviation (width) of the light sheet.

We can find the excitation kernel for path A by swapping the x and z coordinates in Eq. 3. This is a simple modification for the spatial part of the excitation kernel (change $\mathfrak{g}(r_x, \sigma_{\mathrm{ls}})$ to $\mathfrak{g}(r_z, \sigma_{\mathrm{ls}})$), and the coefficients of

the spherical harmonics are transformed by a matrix multiplication

$$\begin{bmatrix} c'^{0}_{0} \\ c'^{-2}_{2} \\ c'^{-1}_{2} \\ c'^{0}_{2} \\ c'^{1}_{2} \\ c'^{2}_{2} \end{bmatrix} = \begin{bmatrix} 1 & 0 & 0 & 0 & 0 & 0 \\ 0 & 0 & -1 & 0 & 0 & 0 \\ 0 & -1 & 0 & 0 & 0 & 0 \\ 0 & 0 & 0 & -1/2 & 0 & \sqrt{3}/2 \\ 0 & 0 & 0 & 0 & 1 & 0 \\ 0 & 0 & 0 & \sqrt{3}/2 & 0 & 1/2 \end{bmatrix} \begin{bmatrix} c^{0}_{0} \\ c^{-2}_{2} \\ c^{-1}_{2} \\ c^{0}_{2} \\ c^{1}_{2} \\ c^{2}_{2} \end{bmatrix}, \tag{4}$$

where c_l^m is coefficient of the y_l^m spherical harmonic in the original frame and c'^m_l is the coefficient of the same spherical harmonic in the rotated frame. Applying this transformation gives

$$h_{\mathrm{A,exc}}(\mathfrak{r}_o, \hat{\mathbf{s}}_o; \hat{\mathbf{p}}) = \Bigg[z_0^{\mathrm{A}}(\hat{\mathbf{p}}) y_0^0(\hat{\mathbf{s}}_o) + \sqrt{\frac{3}{5}} z_{-2}^{\mathrm{A}}(\hat{\mathbf{p}}) y_2^{-1}(\hat{\mathbf{s}}_o) + \frac{1}{2\sqrt{5}} \left\{ 3 z_2^{\mathrm{A}}(\hat{\mathbf{p}}) - z_0^{\mathrm{A}}(\hat{\mathbf{p}}) \right\} y_2^0(\hat{\mathbf{s}}_o) + \frac{1}{2}\sqrt{\frac{3}{5}} \left\{ z_2^{\mathrm{A}}(\hat{\mathbf{p}}) - z_0^{\mathrm{A}}(\hat{\mathbf{p}}) \right\} y_2^2(\hat{\mathbf{s}}_o) \Bigg] \mathfrak{g}(r_z, \sigma_{\mathrm{ls}}). \tag{5}$$

Notice that we have used a different set of circular harmonics for each view. The $z_n^{\mathrm{B}}(\hat{\mathbf{p}})$ circular harmonics are defined by the angle to the x-axis from the $+y$-axis direction, and the $z_n^{\mathrm{A}}(\hat{\mathbf{p}})$ circular harmonics are defined by the angle to the z-axis from the $+y$-axis direction. This change of definition follows directly from swapping the x and z coordinates to go from path B to path A.

In the paper draft we derive the two-dimensional detection kernel. Note that this model differs from the May 14 model—the old model contains an error that over predicts the spatio-angular coupling by a factor of 4. The kernel is two-dimensional because it only considers thin in-focus objects. For a complete non-paraxial three-dimensional model I would eventually like to follow Backer and Moerner [1], but there is still a few weeks of work required to find the associated transfer functions. Instead I'll follow the early diSPIM deconvolution models [2] and use an axial Gaussian function to model the detection kernel.

The detection kernel for an objective along the z axis (path A) as

$$h_{\mathrm{A,det}}(\mathfrak{r}_o, \hat{\mathbf{s}}_o) = \left\{ \left[a_1(r_{xy}) + \frac{\alpha^2}{4} a_2(r_{xy}) \right] y_0^0(\hat{\mathbf{s}}_o) + \frac{1}{\sqrt{5}} \left[-a_1(r_{xy}) + \frac{\alpha^2}{2} a_2(r_{xy}) \right] y_2^0(\hat{\mathbf{s}}_o) \right\} \mathfrak{g}(r_z, \sigma_{\mathrm{det}}), \tag{6}$$

where

$$a_n(r) \equiv \frac{n}{\pi} \left[\frac{J_n(2\pi\nu_o r)}{2\pi\nu_o r} \right], \tag{7}$$

and

$$r_{xy} \equiv \sqrt{r_x^2 + r_y^2}, \qquad \nu_o \equiv \frac{\mathrm{NA}}{\lambda}, \qquad \alpha \equiv \frac{\mathrm{NA}}{n_0}. \tag{8}$$

To find the two-dimensional detection kernel for path B we transform the spherical harmonic coefficients using Eq. 4

$$h_{\mathrm{B,det}}(\mathfrak{r}_o, \hat{\mathbf{s}}_o) = \Bigg\{ \left[a_1(r_{yz}) + \frac{\alpha^2}{4} a_2(r_{yz}) \right] y_0^0(\hat{\mathbf{s}}_o) + \frac{1}{2\sqrt{5}} \left[-a_1(r_{yz}) + \frac{\alpha^2}{2} a_2(r_{yz}) \right] y_2^0(\hat{\mathbf{s}}_o) + \frac{1}{2}\sqrt{\frac{3}{5}} \left[-a_1(r_{yz}) + \frac{\alpha^2}{2} a_2(r_{yz}) \right] y_2^2(\hat{\mathbf{s}}_o) \Bigg\} \mathfrak{g}(r_x, \sigma_{\mathrm{det}}), \tag{9}$$

where $r_{yz} \equiv \sqrt{r_y^2 + r_z^2}$.

The complete kernel is the product of the excitation and detection kernels

$$h_{\mathrm{v}}(\mathfrak{r}_o, \hat{\mathbf{s}}_o; \hat{\mathbf{p}}) = h_{\mathrm{v,exc}}(\mathfrak{r}_o, \hat{\mathbf{s}}_o; \hat{\mathbf{p}}) h_{\mathrm{v,det}}(\mathfrak{r}_o, \hat{\mathbf{s}}_o). \tag{10}$$

Notice that the both the excitation and detection kernels are Gaussian along the axial detection axis, so the complete kernel is also Gaussian along that dimension with standard deviation $\sigma_{\mathrm{ax}} = \sqrt{\sigma_{\mathrm{ls}}^2 + \sigma_{\mathrm{det}}^2}$. Therefore, we can rewrite the kernel in the form

$$h_{\mathrm{A}}(\mathfrak{r}_o, \hat{\mathbf{s}}_o; \hat{\mathbf{p}}) = \left[\sum_{l=0}^{\infty} \sum_{m=-l}^{l} \sum_{n=-\infty}^{\infty} h_{l,n,\mathrm{A}}^m(r_{xy}) y_l^m(\hat{\mathbf{s}}_o) z_n(\hat{\mathbf{p}}) \right] \mathfrak{g}(r_z, \sigma_{\mathrm{ax}}), \tag{11}$$

$$h_{\mathrm{B}}(\mathfrak{r}_o, \hat{\mathbf{s}}_o; \hat{\mathbf{p}}) = \left[\sum_{l=0}^{\infty} \sum_{m=-l}^{l} \sum_{n=-\infty}^{\infty} h_{l,n,\mathrm{B}}^m(r_{yz}) y_l^m(\hat{\mathbf{s}}_o) z_n(\hat{\mathbf{p}}) \right] \mathfrak{g}(r_x, \sigma_{\mathrm{ax}}). \tag{12}$$

3 Transfer function

We can rewrite Eqs. 1 and 2 in the frequency domain as

$$G_{\mathrm{v},n}(\boldsymbol{\nu}) = \sum_{l=0}^{\infty} \sum_{m=-l}^{l} H_{l,n,\mathrm{v}}^m(\boldsymbol{\nu}) F_l^m(\boldsymbol{\nu}), \tag{13}$$

$$F_l^m(\boldsymbol{\nu}) = \sum_{\mathrm{v} \in \{\mathrm{A,B}\}} \sum_{n=-\infty}^{\infty} H_{l,n,\mathrm{v}}^m(\boldsymbol{\nu}) G_{\mathrm{v},n}(\boldsymbol{\nu}), \tag{14}$$

where

$$G_{\mathrm{v},n}(\boldsymbol{\nu}) = \int_{\mathbb{R}^3} d\mathfrak{r}_d \, \mathrm{e}^{i2\pi \mathfrak{r}_d \cdot \boldsymbol{\nu}} \int_{\mathbb{S}^1} d\hat{\mathbf{p}} \, z_n(\hat{\mathbf{p}}) g_{\mathrm{v}}(\mathfrak{r}_d, \hat{\mathbf{p}}), \tag{15}$$

$$H_{l,n,\mathrm{v}}^m(\boldsymbol{\nu}) = \int_{\mathbb{R}^3} d\mathfrak{r}_o \, \mathrm{e}^{i2\pi \mathfrak{r}_o \cdot \boldsymbol{\nu}} \int_{\mathbb{S}^1} d\hat{\mathbf{p}} \, z_n(\hat{\mathbf{p}}) \int_{\mathbb{S}^2} d\hat{\mathbf{s}}_o \, y_l^m(\hat{\mathbf{s}}_o) h_{\mathrm{v}}(\mathfrak{r}_o, \hat{\mathbf{p}}, \hat{\mathbf{s}}_o), \tag{16}$$

$$F_l^m(\boldsymbol{\nu}) = \int_{\mathbb{R}^3} d\mathfrak{r}_o \, \mathrm{e}^{i2\pi \mathfrak{r}_o \cdot \boldsymbol{\nu}} \int_{\mathbb{S}^2} d\hat{\mathbf{s}}_o \, y_l^m(\hat{\mathbf{s}}_o) f(\mathfrak{r}_o, \hat{\mathbf{s}}_o). \tag{17}$$

In Figs. 1 and 2 we plot the transverse part of the diSPIM transfer function. Extending these plots to three dimensions is simple given our assumption that the axial part is Gaussian. Notice that view B has a non-zero element in the $m = -1$ column—this is a first for the microscopes we've considered so far. Also notice that each view contributes new information—we'll see this result in a clearer form when we find the complete SVD.

4 Single-view singular value decomposition

We'll start by looking at the singular value decomposition of each view by itself. We have already developed all of the tools we need for this computation in the May 14 notes, so we will jump straight to the results.

Figures 3 and 4 show the singular systems for the two individual views of the diSPIM. As we'd expect, the object space singular functions for the two views are identical except for a swap of the x and z axes. From the object space singular functions in the second and third branches of both views, we can see each view is most sensitive to orientations perpendicular to the illumination optical axis—this is what we'd expect for a polarized illumination microscope.

Also notice that uniform distributions (or anything resembling a uniform distribution) are not object-space singular functions of either view. We saw the same thing for single-view epi-illumination microscopes, although

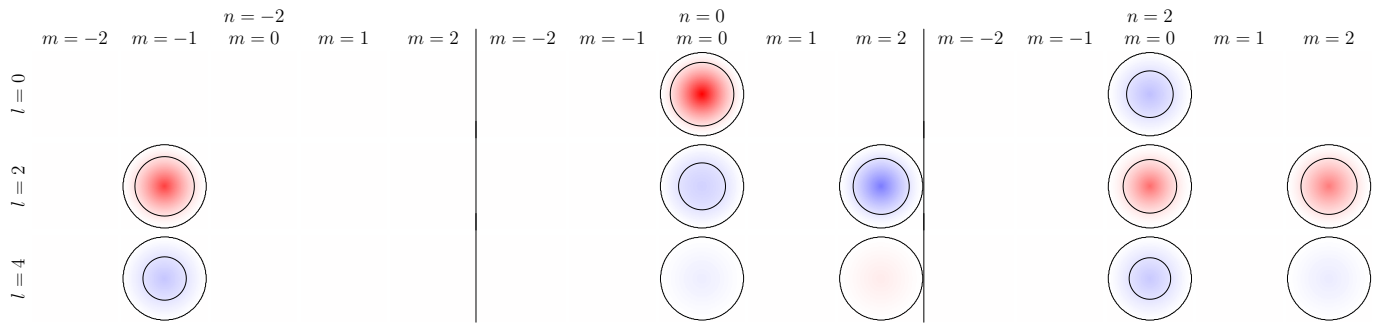

Figure 1: Transverse transfer function $H^m_{l,n,\mathrm{A}}(\boldsymbol{\nu}_{xy})$ for view A of a polarized diSPIM microscope with a 0.8 NA detection objective. **Rows:** l indexes the object-space spherical harmonic band. **Columns:** m indexes the object-space spherical harmonic degree, and n indexes the data-space circular harmonic band. **Entries:** Each column and row contains a continuous two-dimensional plot indexed by the vector $\boldsymbol{\nu}_{xy}$ ranging from $-2\mathrm{NA}/\lambda$ to $+2\mathrm{NA}/\lambda$ (although $\boldsymbol{\nu}_{xy}$ is rotationally symmetric so one dimension would suffice). All values are normalized between -1 (blue) and $+1$ (red) with 0 colored white.

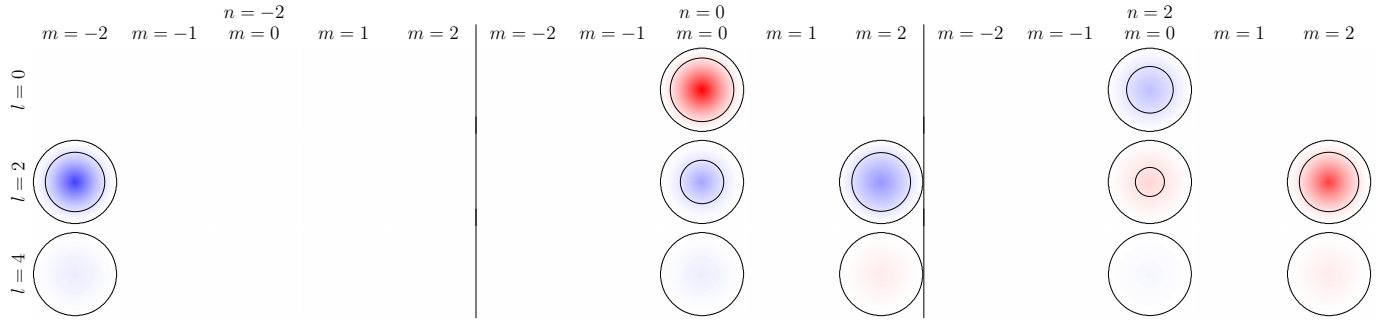

Figure 2: Transverse transfer function $H^m_{l,n,\mathrm{B}}(\boldsymbol{\nu}_{yz})$ for view B of a polarized diSPIM microscope with a 0.8 NA detection objective. See caption of Fig. 1 for details.

in that case there were object-space singular functions that were mostly uniform with slight depressions along the optical axis. Note that we can still measure uniform distributions with either view, but these distributions have a component in the null space.

5 Dual-view singular value decomposition

We will follow Burvall et al. [3] and the single-view case and calculate the singular value decomposition in data space. We want to find the eigenvalues $\mu_{\boldsymbol{\rho},j}$ and eigenfunctions $v_{\boldsymbol{\rho},j,\mathrm{v}}(\mathfrak{r}_d, \hat{\mathbf{p}})$ that satisfy

$$[\mathcal{H}\mathcal{H}^\dagger \mathbf{v}_{\boldsymbol{\rho},j}]_\mathrm{v}(\mathfrak{r}_d, \hat{\mathbf{p}}) = \mu_{\boldsymbol{\rho},j} v_{\boldsymbol{\rho},j,\mathrm{v}}(\mathfrak{r}_d, \hat{\mathbf{p}}). \tag{18}$$

In the frequency domain the data-space singular functions will be in the form

$$v_{\boldsymbol{\rho},j,\mathrm{v}}(\mathfrak{r}_d, \hat{\mathbf{p}}) = \mathrm{e}^{i2\pi\boldsymbol{\rho}\cdot\mathfrak{r}_d} \sum_{n=-\infty}^{\infty} [V_{n,\mathrm{v}}(\boldsymbol{\rho})]_j \, z_n(\hat{\mathbf{p}}). \tag{19}$$

Plugging Eqs. 13, 14, and 19 in 18 gives

$$\sum_{n=-\infty}^{n=\infty} \sum_{\mathrm{v}\in\{\mathrm{A},\mathrm{B}\}} \sum_{l=0}^{\infty} \sum_{m=-l}^{l} H^m_{l,\mathrm{v}',n'}(\boldsymbol{\rho}) H^m_{l,\mathrm{v},n}(\boldsymbol{\rho}) \, [V_{n,\mathrm{v}}(\boldsymbol{\rho})]_j = \mu_{\boldsymbol{\rho},j} \, [V_{n,\mathrm{v}}(\boldsymbol{\rho})]_j \, . \tag{20}$$

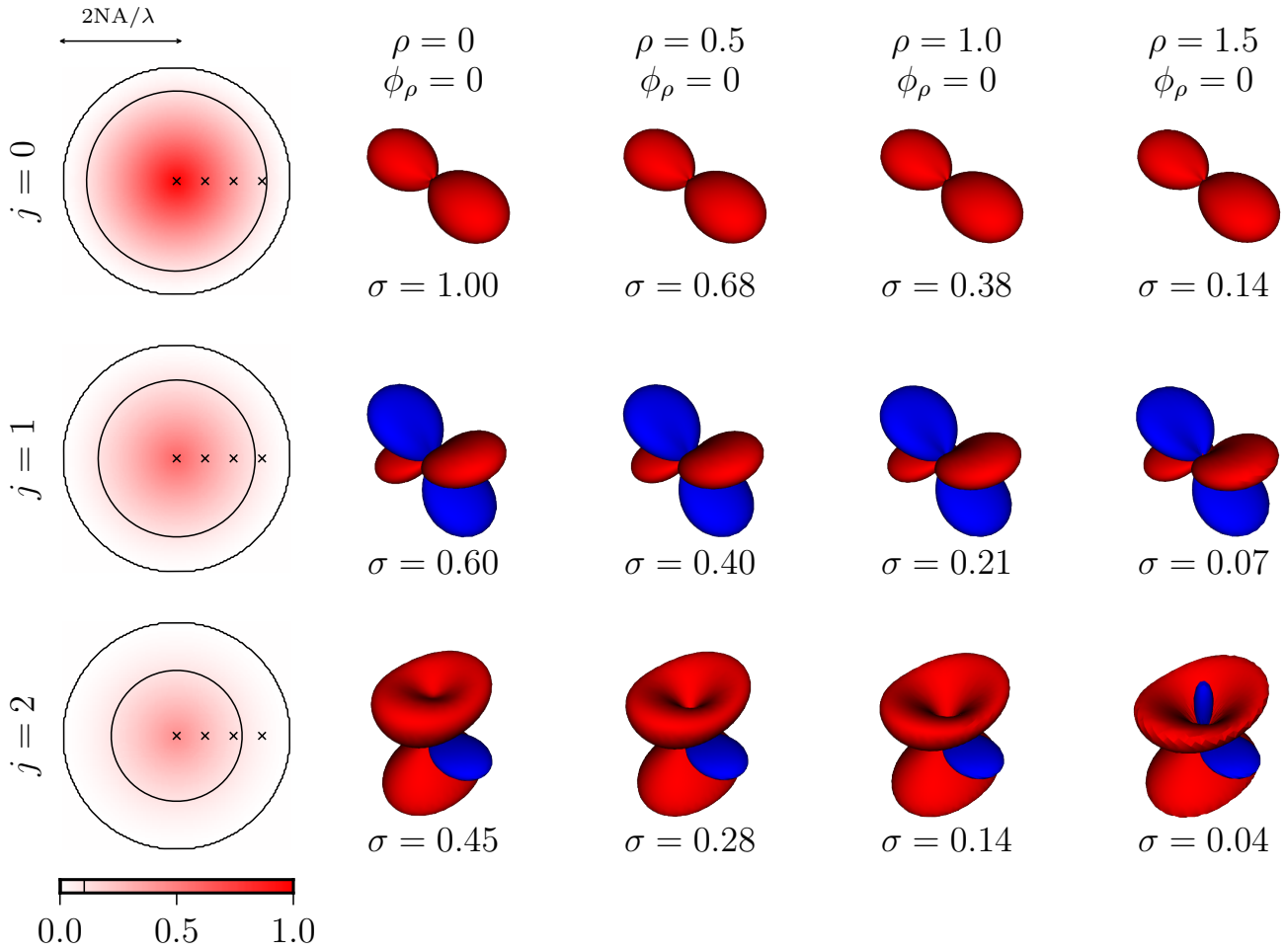

Figure 3: Singular system for view A (x-illumination, z-detection) of a polarized diSPIM microscope with a 0.8 NA detection objective. **Rows:** Discrete branches of the singular value system indexed by j. **Column 1:** Continuous singular value spectrum for each branch j indexed by spatial frequency $\boldsymbol{\rho}$. The singular value spectra are normalized with contour lines at 0 and 0.1. **Columns 2-5:** Angular part of the object-space singular vector at spatial frequencies marked with 'x's in the first column. The camera is facing the origin along the [1,1,1] axis with the z axis pointing up along the page. A red surface indicates positive values, a blue surface indicates negative values, and the distance from the origin indicates the magnitude.

If we combine the indices n and v into a multi-index $\mathbf{i} = (n, \mathrm{v})$ then we can rewrite 20 as

$$\sum_{\mathbf{i}} \left[\sum_{l=0}^{\infty} \sum_{m=-l}^{l} H^m_{l,\mathbf{i}'}(\boldsymbol{\rho}) H^m_{l,\mathbf{i}}(\boldsymbol{\rho}) \right] [V_{\mathbf{i}}(\boldsymbol{\rho})]_j = \mu_{\boldsymbol{\rho},j} \, [V_{\mathbf{i}}(\boldsymbol{\rho})]_j \, . \tag{21}$$

Finally, we can rewrite Eq. 21 in matrix form as

$$\mathsf{K}(\boldsymbol{\rho}) \mathsf{V}_j(\boldsymbol{\rho}) = \mu_{\boldsymbol{\rho},j} \mathsf{V}_j(\boldsymbol{\rho}), \tag{22}$$

where the entries of $\mathsf{K}(\boldsymbol{\rho})$ are given by

$$K_{\mathbf{i},\mathbf{i}'}(\boldsymbol{\rho}) = \sum_{l=0}^{\infty} \sum_{m=-l}^{l} H^m_{l,\mathbf{i}'}(\boldsymbol{\rho}) H^m_{l,\mathbf{i}}(\boldsymbol{\rho}). \tag{23}$$

For the diSPIM, the matrix K has 6×6 non-zero entries—two views with three circular harmonics for each view—so solving this eigenvalue problem at each point in frequency space is computationally feasible.

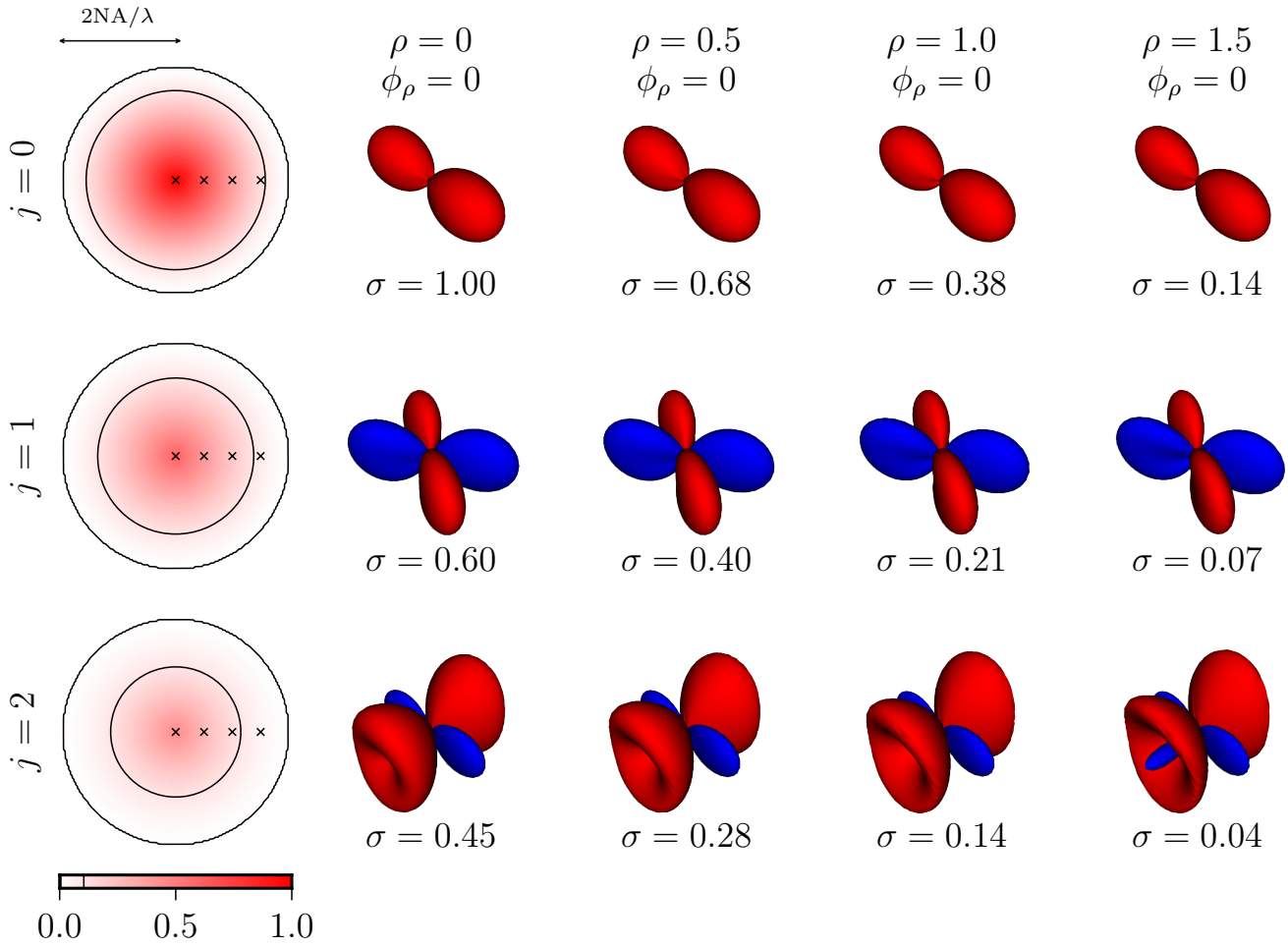

Figure 4: Singular system for view B (z-illumination, x-detection) of a polarized diSPIM microscope with a 0.8 NA detection objective. See Fig. 3 caption for details.

Figures 5–7 show the singular systems for a symmetric 0.8 NA polarized illumination diSPIM microscope where the axial resolution ($\propto 1/\sigma_{\text{ax}}$) is 1/3 of the lateral resolution for each view. I expect to modify this parameter based on bead measurements taken with the final system.

References

[1] Adam S. Backer and W. E. Moerner. Extending single-molecule microscopy using optical Fourier processing. *J. Phys. Chem. B*, 118(28):8313–8329, 2014.

[2] Yicong Wu, Peter Wawrzusin, Justin Senseney, Robert Fischer, Ryan Christensen, Anthony Santella, Andrew G. York, Peter W. Winter, Clare M. Waterman, Zhirong Bao, Daniel Colón-Ramos, Matthew McAuliffe, and Hari Shroff. Spatially isotropic four-dimensional imaging with dual-view plane illumination microscopy. *Nature Biotechnology*, 31:1032–1038, 2013.

[3] Anna Burvall, Harrison H. Barrett, Christopher Dainty, and Kyle J. Myers. Singular-value decomposition for through-focus imaging systems. *J. Opt. Soc. Am. A*, 23(10):2440–2448, Oct 2006.

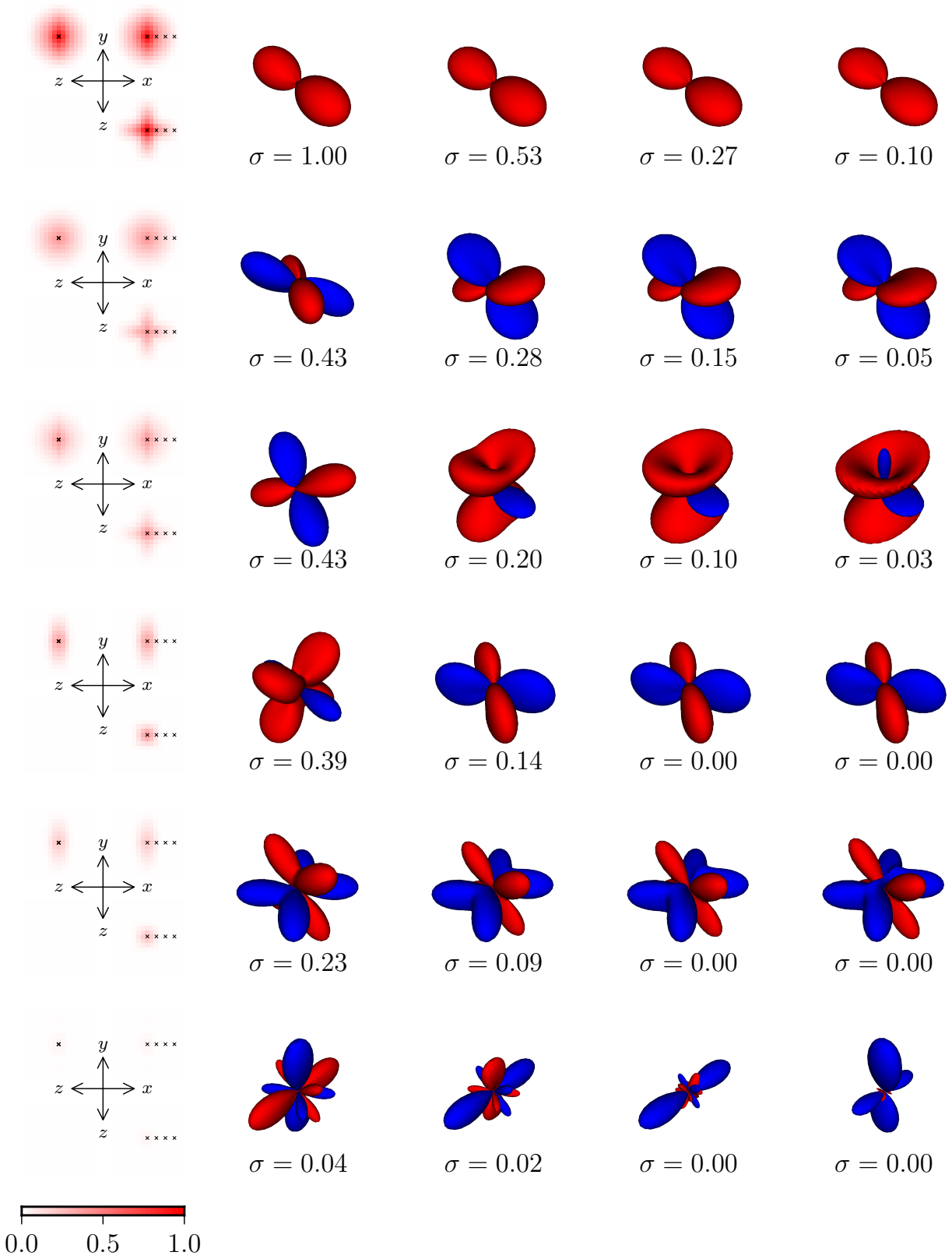

Figure 5: Singular system for a symmetric 0.8 NA polarized illumination diSPIM microscope. **Rows:** Discrete branches of the singular value system. **Column 1:** Maximum intensity projections of the normalized singular value spectrum for each branch indexed by 3D spatial frequency $\boldsymbol{\rho}$. **Columns 2-5:** Angular part of the object-space singular vector at spatial frequencies marked with 'x's in the first column. The camera is facing the origin along the [1,1,1] axis with the z axis pointing up along the page. A red surface indicates positive values, a blue surface indicates negative values, and the distance from the origin indicates the magnitude.

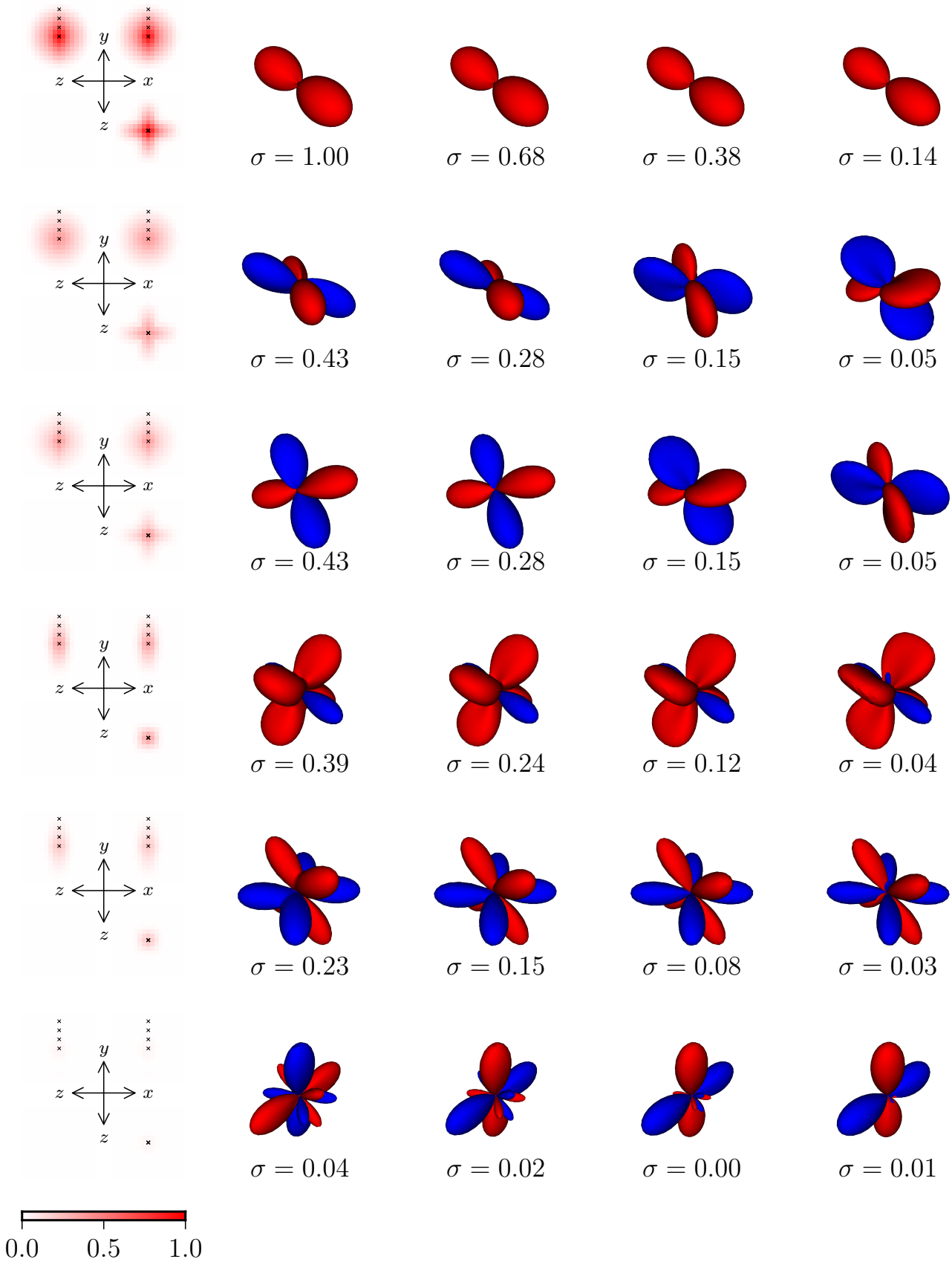

Figure 6: Identical to Figure 5 with object space singular values along the y axis.

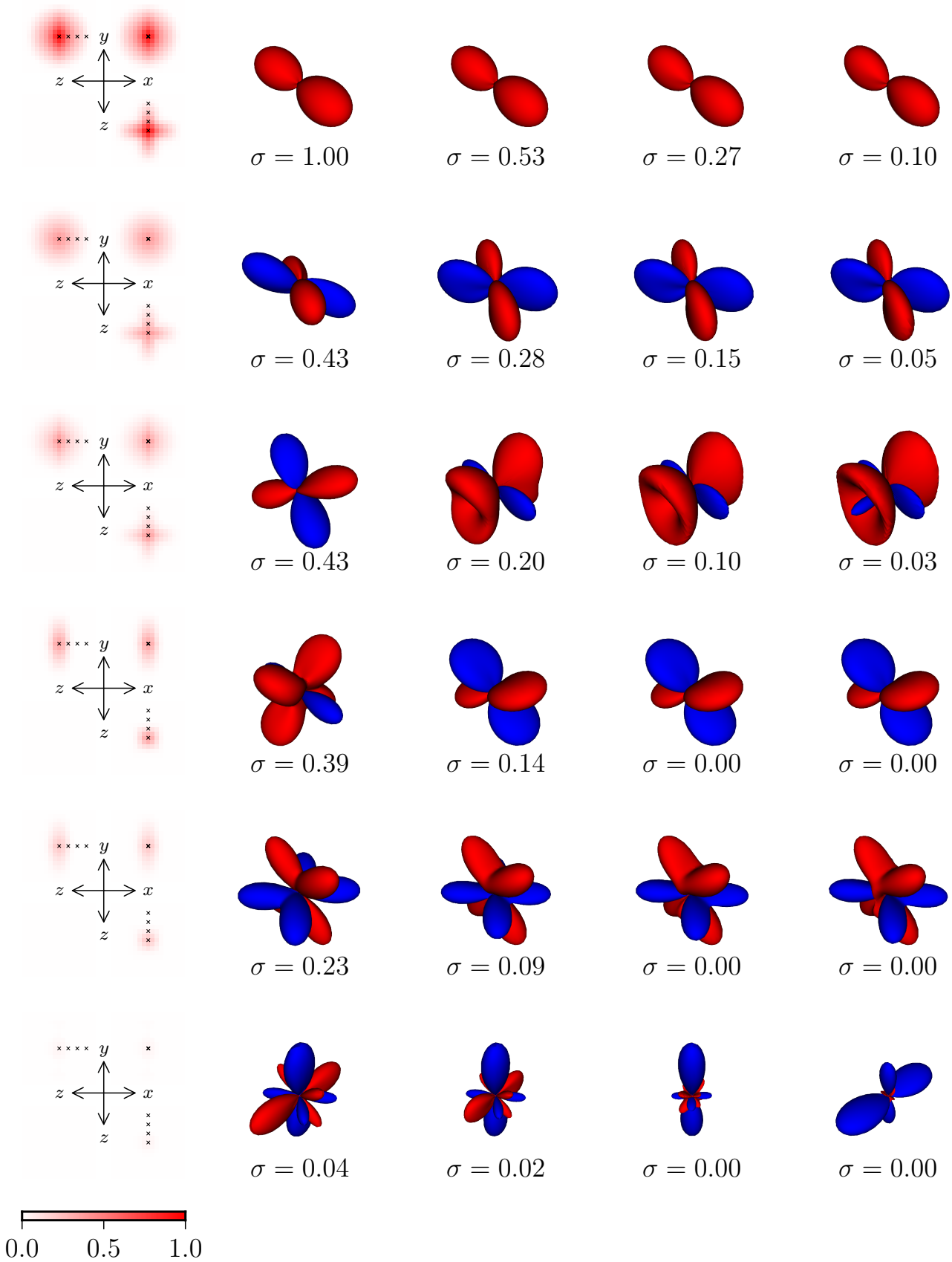

Figure 7: Identical to Figure 5 with object space singular values along the z axis.